CHEMISTRY
A European Journal

A Journal of
ChemPubSoc Europe

Accepted Article

Title: CHEMICAL FUNCTIONISATION OF 2D MATERIALS VIA BATCH AND CONTINUOUS HYDROTHERMAL SYNTHESIS

Authors: Uthman Alli, Sunil J. Hettiarachchi, and Suela Kellici

To be cited as: *Chem. Eur. J.* 10.1002/chem.202000383

Link to VoR: http://dx.doi.org/10.1002/chem.202000383

Supported by
ACES

WILEY-VCH

10.1002/chem.202000383

WILEY-VCH

MINIREVIEW

CHEMICAL FUNCTIONALISATION OF 2D MATERIALS VIA BATCH AND CONTINUOUS HYDROTHERMAL SYNTHESIS

Uthman Alli, Sunil J. Hettiarachchi and Dr Suela Kellici *

Abstract: 2D materials are single or few layered materials consisting of one or several elements with a thickness of a few nanometers. Their unique, tunable physical and chemical properties including ease of chemical functionalization makes this class of materials useful in a variety of technological applications**.** The feasibility of 2D materials strongly depends on better synthetic approaches to improve properties, increase performance and durability and reduce costs. As such, in the synthesis of nanomaterials, hydrothermal processes are widely adopted through a precursor-product synthesis route. This method includes batch or continuous flow systems, both employing water at elevated temperatures (above boiling point) and pressures to fine tune the physical, chemical, optical and electronic properties of the nanomaterial. Both techniques yield particles with different morphology, size and surface area due to different mechanisms of particle formation. In this review, we present batch and continuous hydrothermal synthesis of a selection of 2D derivatives (graphene, MXene and molybdenum disulphide), their chemical functionalisation as an advantageous approach in exploring properties of these materials as well as the benefits and challenges of employing these processes, and an outlook for further research.

Keywords: 2D materials • Hydrothermal synthesis • supercritical fluid • Chemical functionalisation • continuous hydrothermal flow synthesis

1. Two-Dimensional (2D) Materials and Properties

2D materials may consist of a single or a few layers, each layer being one or several atoms thick, with overall layer/s thickness of just a few nanometres[1]. With increasing attention, 2D materials have been explored extensively owing to their ultrathin atomic thickness, tuneable physical and chemical properties **(Fig. 1)** which render their application in many fields such as optical, electrical, chemical and biomedical science[2]. The ability to control the electronic and optical properties of 2D materials is as a result of electrons and electron holes being squeezed into a dimension that is near the exciton Bohr radius[3]. At this critical quantum dimension due to reduction in size (1-100 nm), the band gap increases and thus creating a new property of the material. Some of these 2D materials include Graphene (G), Boron Nitride (BN), MXene, Molybdenum disulphide (MoS_2) and their derivatives. These materials can be classified according to their composition and/or structure.[4] 2D materials can be classified as homo-elemental and hetero-elemental **(Fig. 2)**. Homo-elemental 2D materials include semiconducting black phosphorus (BP) consisting of layers of phosphorus atoms covalently bonded together with Van der Waals interaction between the layers. Other examples of homo-elemental 2D materials include graphene, silicone, antimonene and bismuthene. Hetero-elemental 2D materials include transition metal dichalgonides (TMD's) such as molybdenum disulphide (MoS_2) having covalent bonding between Mo and S atoms and weaker Van der Waals interaction between S atoms making it easy to obtain few layers by mechanical exfoliation. Other examples include boron nitride (BN, white "graphene"), MXenes[5] such as Ti_2C, Ti_3C_2 and $(Ti,V)_2C$. The structures of these 2D materials are shown in **Fig. 2**.

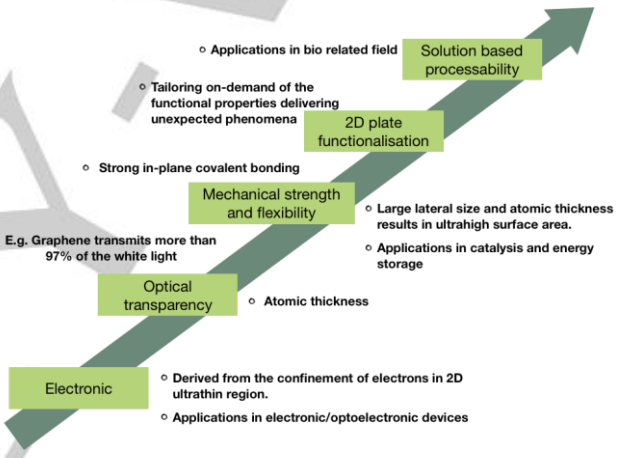

Fig. 1. 2D Materials properties

Structural classification of 2D materials include single layered and multi-layered 2D materials[6–11]. Graphene and MXene are 2D materials with single and multi-layered structures, respectively. Other examples of multi-layered 2D materials are molybdenum disulphide, boron nitride and black phosphorus.

1.1. Graphene

Graphene (G), probably the most recognisable of the 2D materials, is a flat monolayer of sp^2 carbon atoms tightly packed into a 2D honeycomb lattice. It can be transformed into other dimensions such as 0D, 1D and 3D, which are fullerenes or quantum dots, nanotubes and graphite respectively[12] **(Fig. 2)**. Graphene serves as a building block for these dimensions of graphitic materials. Graphene has remarkable electronic properties which has made its research in the electronic/optolectronic industry very promising. Graphene is a zero-band semi-conductor due to the overlapping nature of its valence and conducting bands. It also exhibits a 2.3% absorption in the white light spectrum. With a high theoretical specific surface area of approximately 2630 $m^2\ g^{-1}$, graphene provides an electrochemical double layer gravimetric capacitance[13] of about 550 $F\ g^{-1}$. Despite these exciting properties of graphene, the hydrophobic nature of graphene affects its application in certain fields such as biomedicine. This is due to Van der Waals interactions and π-π stacking between its aromatic

Uthman Alli, Sunil Jayantha Hettiarachchi and Dr Suela Kellici
School of Engineering
London South Bank University
103 Borough Road, London, SE1 0AA, United Kingdom
Email: alliu@lsbu.ac.uk, hettiars@lsbu.ac.uk, *kellicis@lsbu.ac.uk,
Web:www.nano2d.co.uk

10.1002/chem.202000383

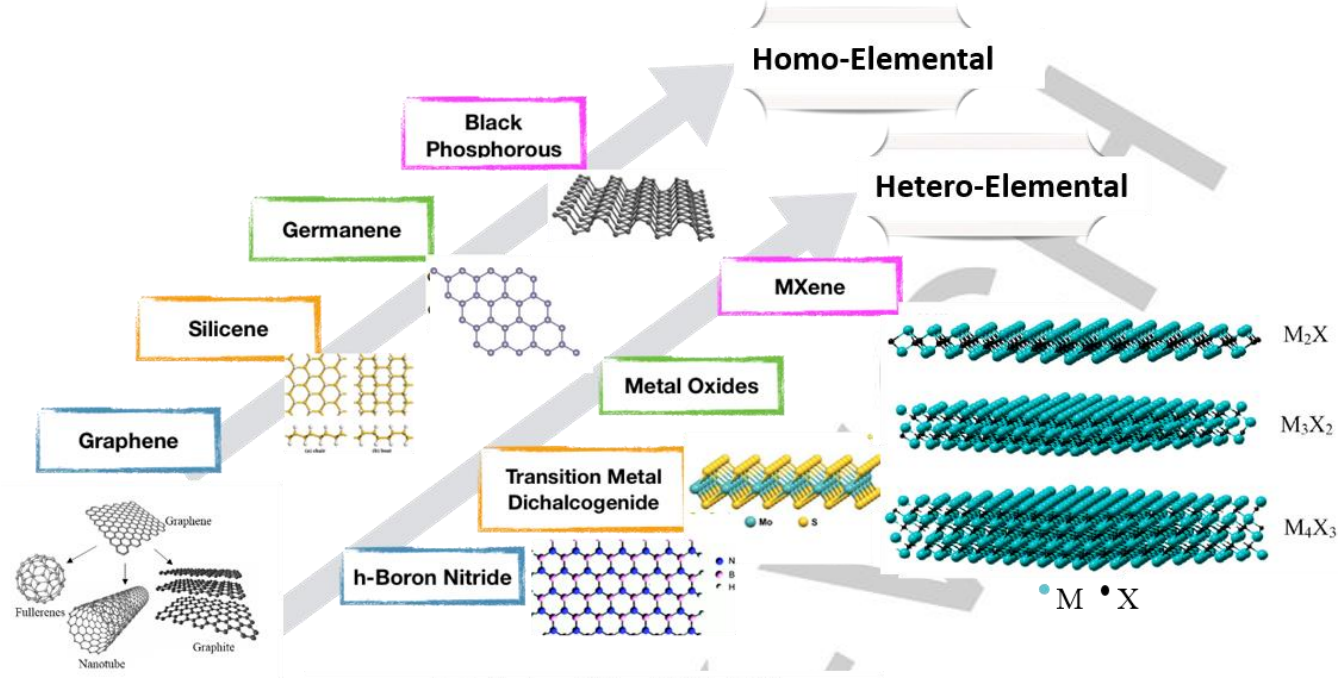

Fig. 2. Structures of different 2D Materials [6-11]

rings which allows graphene to form aggregates in solution. This behaviour could impair its function in areas of biomedical science such as drug deliverability, bio-sensing and bio-imaging[2]. According to Zhang and co-workers, graphene exhibits hydrophobicity unless when it is in its oxidised form as graphene oxide (GO)[14]. As a result, graphene use in certain applications requires addition of polymers or surfactants to be stable in aqueous solutions[14]. Considering its excellent mechanical, electronic and surface properties, graphene is a promising electrode material for energy storage devices..Few proof-of-concept devices have been shown in various applications, however graphene is unlikely to be fully utilized, as alone it does not possess the integrative properties that are required in a range of diverse technological applications. Quality parameters such as surface defects, mechanical deformation and electronic environment as well as the number of graphene layers, (all induced as a result of the synthetic process), profoundly affect the end properties of the material.

1.2. Molybdenum Disulphide MoS_2

Since the introduction of the fascinating graphene, other 2D materials such as molybdenum disulphide have led to an extraordinary renewed interest from both academia and industry. MoS_2, an inorganic analogue of graphene, constitutes to the layered transition metal dichalcogenides group with a formula MX_2 [4]. A single MX_2 layer consists of transition metal atoms from group IV, V or VI such as Molybdenum (Mo) sandwiched by two layers of X, where X is either sulphur (S) or selenium (Se) atoms, through covalent bonding (**Fig. 2**)[15]. The MX_2 layers are held together by weak Van der Waals forces and can be easily separated to single MX_2 nanosheets. This separation facilitates greater surface area, which provides improved contact with electrolyte, hence increasing adsorption of electrolyte ions in energy storage applications[15]. Similar to graphene, MoS_2 is found to exhibit a wealth of distinctive properties such quantum confinement fluorescence (that occur when cutting a MoS_2 monolayer to *ca.* 10 nm), chemical stability, large specific surface area (up to 210 m^2/g)[16] *etc.* In contrast to graphene, which exhibits a zero-band gap, a single sheet of MoS_2 is a direct bandgap semiconductor. It is also noted that as with graphene, the properties of the monolayer MoS_2 are strikingly different from the bulk material, phenomena which is common among the 2D materials.

Uthman has a Bachelor's degree in Chemistry and a Master's degree in Petroleum and Gas Engineering. He is currently enrolled as a PhD research student at London South Bank University and focuses on synthesis and application of 2D materials in energy storage devices.

Dr Kellici is Associate Professor in Materials Engineering and leading the Nano2D group. She has a degree in Chemistry and PhD in Materials Chemistry from Queen Mary University of London followed by a PDRA position at University College London. Dr Kellici is a highly interdisciplinary materials engineer with a passion in designing advanced functional nanomaterials (utilizing a target-oriented approach and clean technologies) that provide effective solutions to global challenges in the energy, biomedical and environmental applications.

Sunil holds a MSc in Engineering from University of Derby, UK and PGD in Mechanical Engineering from City & Guilds of London Institute, UK. His on-going research explores enhancing engine oil performance via addition of nanoparticles and bio lubricants as additives.

The applications of 2D-MoS_2 span from chemical and bio-sensors, bio-tagging, catalysts, supercapacitor, lithium ion batteries to optoelectronics. It can also be utilized as a photocatalytic and photovoltaic material due to its strong absorption of the visible light. 2D-MoS_2 exhibits differences compared with graphene nanosheet including a high thermal and chemical stability high surface area values, thus making it as a very attractive electrode material for electrochemical devices such as lithium ion batteries. The large surface area of MoS_2 provides more active sites for charge storage in electric double layer capacitors. MoS_2 has an interlayer distance of 0.65 nm which promotes ion intercalation for additional capacitance[13]. In addition, the wide range of oxidation state of molybdenum (Mo) offers MoS_2 a pseudo-capacitive mechanism of charge storage. Crystal phases of bulk MoS_2 exists as thermodynamically stable 2H phase and metastable 1T phase. The 2H phase exhibits a hexagonal symmetry for its crystal structure whilst the 1T phase shows a trigonal symmetry of its crystal structure. These two phases have different electronic properties due to the difference in their crystal symmetry[6].
2D MoS_2 can be synthesised by chemical vapour deposition (CVD)[17], hydrothermal synthesis[18] and exfoliation methods[17]. CVD offers high quality MoS_2 nanosheets but the methodology is quite expensive and offers low productivity. The first continuous hydrothermal flow synthesis of MoS_2 was reported by Dunne and co-workers in 2015 where MoS_2 nanosheets were produced by sulphidation of molybdate anions and in flow acidification to amorphous MoS_3 which transformed into MoS_2 nanosheets on further hydrothermal treatment[19].

Despite the extraordinary properties of these materials and the latest efforts in synthetic procedures, in comparison to graphene, the area of inorganic 2D materials still remains hugely unexplored. This clearly is evidenced by the relatively smaller number of research publications which is considered to be primary due to the fact that making the materials with well-defined distinct properties (monolayer and free of defects as well as functionalisating) in a economical, environmentally benign and controlled manner remains challenging.

1.3. MXene

MXenes, first reported in 2011 by Gogotsi and co-workers[20] are described as transition metal carbides, carbonitrides and nitrides obtained by selectively etching out the A element from its MAX phase precursor[5,20]. MAX phase is a bulk material where M stands for an early transition metal (such as Ti, V, Cr, etc.), A is a group IIIA or group IVA element (such as Al or Ga), and X is carbon (C) or carbonitride (CN) or nitride (N). MAX phases (60 so far) can be made with various combinations, and their properties can be altered *via* tuning of their elemental composition.

MXenes have a general formula of $M_{n+1}X_nT_x$, where n = 1, 2 or 3, T_x = surface terminations such as O, OH or F, and x is the number of surface terminations[5]. Some examples are $Ti_3C_2T_x$, Ti_2CT_x, Ti_3CNT_x, $Nb_4C_3T_x$, etc. MXenes exhibit a sandwich-like arrangement, where n+1 layers of M cover n layers of X, i.e $[MX]_n$ M. $Ti_3C_2T_x$ is the most studied MXene with a high electronic conductivity of about 9880 S cm^{-1} and excellent charge-storage properties[21]. MXenes with more than one M element exists **(Fig.1)** in random and ordered arrangements of M atoms. When there is a random arrangement of two different transition metals in the M layers, it is referred to as a solid solution. On the other hand, when the different M atoms are arranged in an orderly manner in the M layer, it is called an ordered phase[5]. MXenes are implored in numerous applications such as electrochemical energy storage, transport conductors, water desalination, antibacterial films, coatings and biosensors[14].

MXene is hydrophilic and has a high electronic conductivity, which allows its electrode to be used as both the active material and current collector in supercapacitors[5]. MXenes also exhibit a pseudo-capacitance through reversible redox reactions occurring at the Ti surface. MXene nanosheets have negative charge which allows formation of stable, viscous aqueous colloidal solution without addition of surfactant and polymer[5,14,21]. In addition, MXene have a higher tap density of about 4 g cm^{-3} as compared to graphene which has a tap density of about 0.4 g cm^{-3}. This property contributes to a higher areal or volumetric capacitance. MXene films also exhibit a high volumetric capacitance of 900 F cm^{-3} [22]. These values show reason for increasing interests in the application of MXenes in energy storage devices.

The novel properties of these 2D nanomaterials are attainable depending on the route of synthesis implored to offer unique characteristics such as high surface area to volume ratio, distinct morphologies and surface functionalities. Several applications of inorganic nanomaterials exploit its particle size variability and surface modifications. Size tuning creates changes to the structure of the material. This includes an increase or decrease in surface area and defects of the material, causing a change in its electronic/optoelectronic properties[23]. Material properties can also be fine-tuned by varying the particle size, thickness and shape, providing use in biomedical applications for example[24].

However, as with previously described 2D materials, standing alone 2D materials do not possess the properties that would fulfil diverse spectrum of potential applications and so optimization/enhancement is required. By utilising the 2D-platelike substrate, it is possible to design new 2D based functional materials with enhanced superior, new and tuneable properties from parent 2D material achievable via chemical and covalent approaches. These creative synthetic protocols create diverse possibilities for new/improved/enhanced unexpected phenomena.

2. Synthetic methodologies of 2D Materials

The 2D material structure of these nanosheets allows for the engineering of 2D based materials with new tunable properties. Functionalisation can proceed via different conventional methods, which are classified distinctively according to the processes involved in creating nanometre sized structures. These are the top-down (exfoliation of parent 3D) and bottom-up synthesis (atom-by-atom growth). These methods include; micromechanical exfoliation (exfoliation of layered Van der Waals solids into one or few-layer nanosheets e.g. scotch-tape exfoliation of graphene), ultrasonic exfoliation (use of sound energy to delaminate Van der Waals solids into single or few-layer nanosheets), ion-change exfoliation (for layered ionic solids via proton-exchange reactions in aqueous solutions), template synthesis (growing crystals on a template into required dimension), microwave-assisted synthesis (by microwave irradiation of materials), topochemical transformation (nucleation and growth of particles inside the precursors to retain their morphology), chemical vapour deposition (high temperature deposition of materials on substrate) and hydro/solvothermal synthesis[17]. However, this paper only reviews hydrothermal methods of 2D materials synthesis (graphene, MXene and molybdenum disulphide derivatives). Advanced materials refer to chemical substances that are organic and/or inorganic in composition synthesised to achieve desirable physical and chemical properties for a specific application. The objectives therefore involve synthesis, combination and chemical functionisation of 2D materials through hydrothermal processes to achieve desirable properties.

Materials design may include:

- Decorating/functionalising the 2D material with highly crystalline inorganic species, for example homo or hetero metal oxides or metal species.
- Substitutional doping with a selection of heteroatoms such as nitrogen, boron, sulphur, phosporous.
- Coupling with an alternative 2D material, for example molybdenum disulphide and graphene, producing nanocomposite structures.
- Cutting the 2D atomic mat to smaller nanosized materials (<10 nm) to produce 0D quantum dots.
- The as-produced 2D materials can be 3D printed producing structures with improved properties for the target application.

2.1. Hydrothermal synthesis of 2D Materials

The term hydrothermal describes the action of water under elevated temperature and pressure. Byrappa and Yoshimura describes hydrothermal process as any heterogenous reaction occurring in a closed system in the presence of a solvent (aqueous or non-aqueous) at conditions above room temperature and greater than 1 atm[25]. Several terminologies have been used to describe this technology based on the type of solvent used. When non-aqueous solvents are used, it is referred to as solvothermal process and when supercritical fluids are implored, the process is described as supercritical fluid technology[26]. The aforementioned processes are believed to be extensions of the hydrothermal synthesis technology.

Traditional synthesis of solid inorganic nanomaterials involves high-temperature ceramic methods, which limits chemical flexibility and control of particle sizes. Other synthetic methods such as physical and chemical vapour deposition techniques have evolved over the years offering economical and easy routes of nanomaterials production but suffer from environmental concerns raised due to toxicity of precursors used in the process properties[23].

Prior to 1980, in-situ observation of the growth process of particles was not encouraging in analysing the qualities of the materials produced. But today, improvements in hydrothermal reactor designs and availability of advanced analytical techniques such as high-resolution electron microscopy images, Raman and FTIR spectroscopy has helped in in-situ observations of crystal growth, nucleation and materials processing to ultra-fine particles with controllable size and morphology[26]. For example, in situ superheated water crystallisation of nanocystalline ceria particles in the tubing of a continuous hydrothermal flow synthesis (CHFS) mixer was mapped using high-energy synchroton X-ray diffraction[27].

Hydrothermal synthesis is a wet chemical strategy that offers an advantage over commercial material synthesis methods. Improvements such as regulating reaction conditions by adjusting different reaction parameters such as temperature, reactant ratio, reaction time and pressure to generate high product purity and homogeneity with narrow size distributions and lower sintering temperature[17].

Hydrothermal technology has been implored across many disciplines such as chemistry, material science, physics, biology, geology etc., in advanced materials processing and will keep expanding due to the solutions and advantages it offers.

2.2. Batch hydrothermal synthesis (BHS)

The characteristics of density and dielectric constant of near-critical water (NCW) and supercritical water (SCW) have influenced their utility as reaction media[23]. Batch hydrothermal synthesis (BHS) utilizes a reactor similar to an autoclave as used in traditional methods as the reaction environment to produce extremely fine materials[28]. This typically is conducted by heating up precursors at increased pressures and temperatures (above boiling point of water and not higher than 250°C). Specifically, nanoparticles of inorganic single or mixed metal oxides with high crystallinity, large surface area to volume ratio, particle size and morphology to suit many contemporary electromechanical applications[23]. Reactions implicated to the formation of above material such as; hydrolysis and dehydration were explained elsewhere in this document. **Fig. 3.** illustrates a typical batch thermal reactor with the ability to change reaction conditions such as; temperature and pressure of the aqueous solution to synthesis material with desired properties reactor[29]. Agglomeration of nanoparticles is the known disadvantage in this process, as well as reproducibility of material due to batch to batch variations in material properties and long reaction time (hours, days) required for synthesis of materials. Nevertheless, there are many advantages with this process. For example; ability to process material without calcination and milling steps, ability to control oxidation states of the element, thus prepare elements with different oxidation rates etc[30]. BHS has been used to prepare nanomaterials for several applications like catalysis, photovoltaic[32], bio-related[33] and many electromechanical purposes[34].

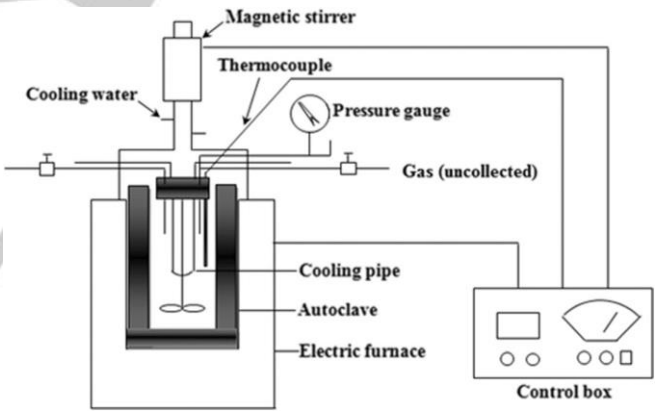

Fig.3. Schematic illustration of a typical hydrothermal batch reactor[29]

2.2.1. 2D Chemical Functionalisation via BHS

Forms of functionalisation involve decorating the surfaces of these 2D materials with compounds to enhance their work function. Such compounds include a range of metals and metal oxides as seen in hydrothermally synthesised MoS_2 modified with ZnO nanoparticles[35], silver wrapped MoS_2[36] for biosensing and energy storage applications respectively. These have been employed in synthesising 2D nanocomposites such as graphene-TiO_2 with application in energy storage[37]. An example of 2D functionalised materials synthesized via BHS is graphene/Mn_3O_4 composites, where $KMnO_4$ and ethylene glycol $(CH_2OH)_2$ served as precursor and reducing agent respectively[38]. As-synthesised nanocomposites were observed to have four times higher capacitance, power density and outstanding capacitance retention upon cycling as compared to Mn_3O_4 nanoparticles. This

could be attributed to the conductivity of graphene sheets to stimulate fast Faradaic charging, discharging of Mn_3O_4 nanorods and the growth of Mn_3O_4 on graphene sheets; avoiding aggregation and providing high surface area between the Mn_3O_4 nanorods and the electrolyte[38]. Other forms of functionalisation include coupling of 2D materials aiming to improve functional properties when compared with the starting 2D parent[39]. This development includes graphene-like MoS_2/graphene (GL-MoS_2/G) composite synthesized via cationic surfactant assisted facile hydrothermal route, with the reduction agents L-cysteine and cetyltrimethylammonium bromide (CTAB). Albeit, it is observed that the increasing CTAB concentration affecting to reduce the layer number of MoS_2 sheets, thus 0.02 mol L^{-1} of CTAB solution demonstrated a higher reversible capacity of 940-1020 mAh g^{-1}, greater cycle stability and a higher rate capability, which may ascribed to effective intercalation of GL-MoS_2 sheets and graphene that optimized the exceptional electrochemical performance for reversible Li^+ storage[39]. Moreover, mesoporous molybdenum disulfide/carbon (MoS_2/C) nanocomposite was synthesized via facile hydrothermal route resulting flower like morphologies. Resulting carbon decorated MoS_2 was with thinner MoS_2 nanosheets with increased specific surface area, thus, enhanced electrochemical properties; specific capacitance of 201.4 F g^{-1} with 0.2 A g^{-1} of current density and long cyclic durability (which are higher than MoS_2 without C decoration), ideal for electrode material of supercapacitors[40].

Chemical functionalisation also extends to incorporating various hetero atoms (such as S, N, B, etc.)[41–44] into the crystal structure of 2D materials *via* doping. An example is the increase in electrochemical capacitance of N-doped MXene electrodes from 34 F g^{-1} to 192 F g^{-1} in the post-etch annealing of MXene in ammonia at temperatures of up to 700°C for 2 hours[44].

BHS can be also be utilised for etching of 2D materials. Examples include MXenes, Ti_3C_2 and Nb_2AlC reported to have higher interlayer distance and large specific surface area, which could affect its accommodation of more cations in between layers. Thus, increasing the storage capacity for supercapacitor application[45]**.** Further, hydrothermal surface functionalisation of MXene also contributes to improving yield of 2D MXene sheets. This was explored by Han et al.,(2019) through hydrothermally assisted intercalation (HAI) of tetramethylammonium hydroxide (TMAOH) between MXene layers to aid its separation into 2D sheets **(Fig. 4)**[46]. This intercalation was also assisted with an antioxidant to protect the surface of MXene from oxidising into TiO_2 nanoparticles. The result gave a high yield of 74% and $Ti_3C_2T_x$ 2D sheets with a high capacitance of 482 F g^{-1} [46]. This provides a direction for mass production of $Ti_3C_2T_x$ 2D sheets and awareness into their optical and electronic properties. MXenes exhibit different surface termination groups; -O, -OH and/or F depending on the choice of etchants used for synthesis. MXenes can be functionalised to have desired termination groups via washing steps with water, high temperature heating or metal adsorption processes[47].

Ultrathin nanoribbons of sodium titanate (M-NTO, $NaTi_{1.5}O_{8.3}$) and potassium titanate (M-KTO, $K_2Ti_4O_9$) were synthesis via facile hydrothermal route, by a simultaneous oxidation and alkalization process of Ti_3C_2 MXene for high performance sodium/potassium ion batteries. The as synthesized M-NTO demonstrated large reversible capacity of 191 mAh g^{-1} at 200 mA g^{-1} for sodium storage and M-KTO exhibited 151 mAh g^{-1} at 50 mA g^{-1} and 88 mAh g^{-1} at a high rate of 300 mA g^{-1} and long term stable cyclability over 900 times, aiding from the interlayer spacing (0.90 and 0.93 nm for M-NTO and M-KTO respectively), ultrafine thickness (< 11 nm), narrow width of nanoribbons (< 60 nm) and open microporous structures for improved ion insertion/extraction kinetics[48].

Development in BHS approaches include the production of selection of quantum dots of molybdenum disulphide[49], graphene[50] and MXene[51]. For instance, graphene quantum dots of *ca.* 10 nm in diameter were synthesised by batch hydrothermal method involving oxidation of graphite and cutting of de-oxidized GO sheets in a furnace at 300°C for 2 h[50]. Also, molybdenum disulfide quantum dots (MoS_2 QDs) were synthesized via BHS route and are with average particle size of 2.8 nm and few layered with narrow size distribution. Thus, the QDs displayed excitation-dependent blue fluorescence because of the polydispersity of the QDs, which could be quenched via photoinduced electron-transfer mechanism for Hyaluronidase (HAase) detection[49]. Moreover, nitrogen-doped MXene (N-Ti_3C_2) with high photoluminescence quantum yield was synthesized via BHS route at 160 ^{0}C, using layered Ti_3C_2 and ethylenediamine as the precursor and the nitrogen source respectively. The as-developed N-MQDs observed to be with 3.4 nm average particle size and enhanced PLQY of up to 18.7%, which proved to be capable of probing ultra-sensitive heavy iron ion (Fe^{3+}) up to detection limit of 100 µm[51].

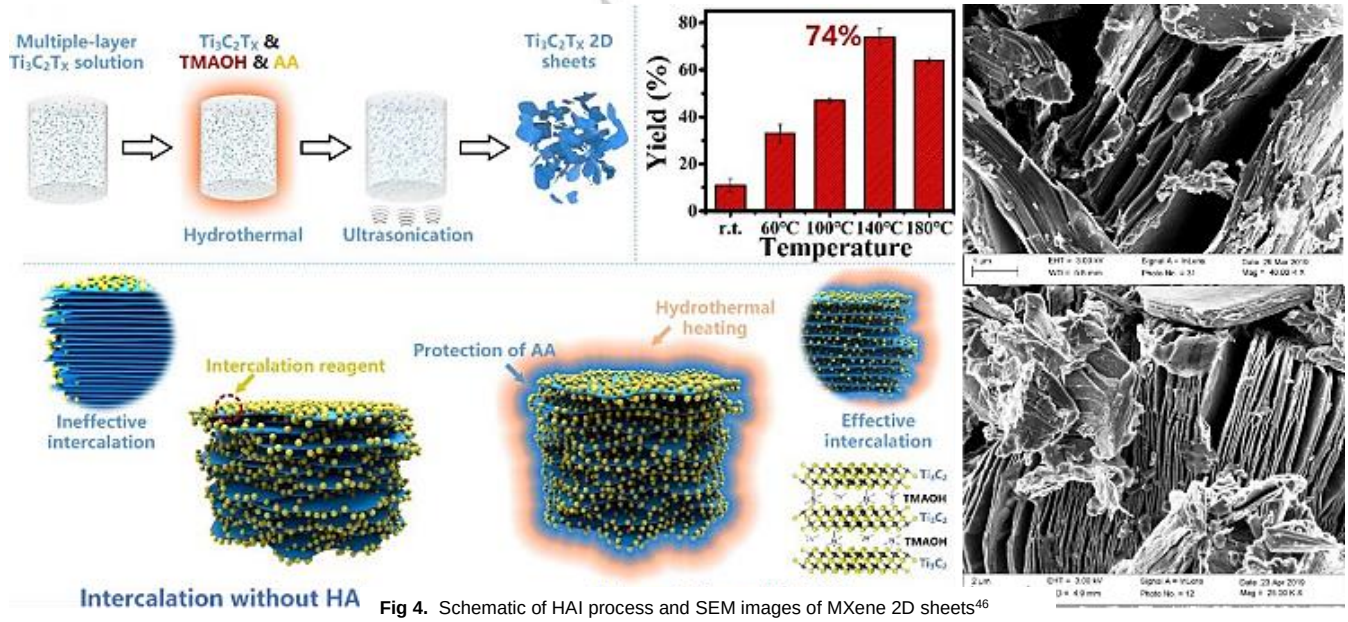

Fig 4. Schematic of HAI process and SEM images of MXene 2D sheets[46]

As stated previously 2D materials exhibits a high specific surface area and the properties (e.g. electrical conductivity) are improved when in its single layer form rather than being stacked up. For example, in graphene re-stacking and agglomeration occur due to π-π* stacking and Van der Waals interaction between unseparated graphene sheets[52]. This can be reduced by addition of hydrophilic or hydrophobic groups (polymers, surfactants and aromatic molecules) between layers to prevent aggregation due to strong polar-polar interactions or steric effects[52,53]. Addition of these groups between graphene layers contributes to their processing into aqueous and non-aqueous dispersions as well as processing into new dimensions[54]. This functionalisation can be achieved using hydrothermal processes or post process (via chemical coupling reactions)[55].

2.3. Continuous Hydrothermal Flow Synthesis (CHFS)

Water is a green solvent whose properties are exploited at supercritical conditions during the hydrothermal synthesis process of 2D materials. The CHFS process involves mixing of aqueous metal salts stream with a flow of supercritical water in a continuous manner within the reactor to produce nano-sized particles[56]. At this supercritical conditions of 374° C and 22.4 MPa, water which is polar behaves like a non-polar solvent due to changes in its density and polarity at high temperatures[23]. Hydrolysis, condensation and thermal decomposition of precursors are reactions occurring at the supercritical water conditions[23]. In the generation of metal oxide nanoparticles, the metal salt hydrolyses, dehydrates and precipitates under set reaction conditions according to **Eqs. (2 - 3)**[57]. These processes occur due to the specific physical and chemical properties of water at these conditions. This behaviour of water and other precursors create an environment that facilitates nucleation and growth of particles[57]. Hydrothermal synthesis of nanoparticles occurs at supercritical conditions where the reaction rate increases due to a decrease in the dielectric constant of supercritical water. Fine particles, metal oxides and single crystals can be synthesised by processing in near- critical or supercritical water conditions by controlling the density, viscosity and dielectric constant of the reaction medium through small changes in temperature and pressure. This offers hydrothermal process an ease to control the particle size, morphology and crystal structure of as-synthesised materials[58].

2.3.1. Properties of supercritical fluid

Supercritical fluids have high compressibility and low viscosity. Water is a polar solvent, this property limits its use in forming soluble solutions with organic and non-polar molecules which may be needed in stabilizing some inorganic nanoparticles[23,58]. Its relatively low boiling point prevents its use in reactions involving high temperature conditions. These limitations can be resolved by achieving a temperature above the boiling point of water when pressure is applied. At a critical condition above 374°C and 22.4 MPa, the polarity and density of water decreases and unusual properties of water is exhibited. Water becomes an excellent solvent for non-polar molecules in this supercritical state due to its reduced dielectric constant and hydrogen-bonding[23]. When cations are in solution, the bond length of M-O (water) is shorter than H-O bond length of water molecules, favouring possible reactions between the metal and water.

$$K_w = [H^+]\,[OH^-] = 1.0e^{-14}\ mol^2\ dm^{-6} \quad (1)$$

$$\text{Hydrolysis:} \quad ML_x + xH_2O \longrightarrow M(OH)_x + xHL \quad (2)$$

$$\text{Dehydration:} \quad M(OH)_x \longrightarrow MO_{x/2} + (x/2)\,H_2O \quad (3)$$

Water has a pH of 7 due to the concentration of $[H^+]$ ions and a dissociation constant (K_w) of $1.0e^{-14}$ mol^2 dm^{-6} at room temperature **(Fig. 5)**. As temperature increases **(Fig.5b)**, it is observed that water at 250°C shows a higher K_w of $1.0e^{-11}$ mol^2 dm^{-6} [23], which is a 30-fold increase in the individual concentration of $[H^+]$ and $[OH^-]$ ions[58]. As a result, there is a strong hydrolysing environment created which facilitates metal hydrolysis when it meets with a flow of supercritical water. The properties of super-critical water such as its reduced dielectric constant and increased dissociation to H^+ and OH^- facilitates the rapid synthesis of various metal oxides. Due to a high concentration of OH^- in this critical state, the metal salt hydrolyses **(eq.2)** and dehydrates **(eq.3)** to generate the metal oxide and precipitates out as nanoparticles[57]. Despite these exciting properties of supercritical water, its miscibility with oxygen and organic solvents presents a reactive environment which can be potentially explosive in extreme conditions.

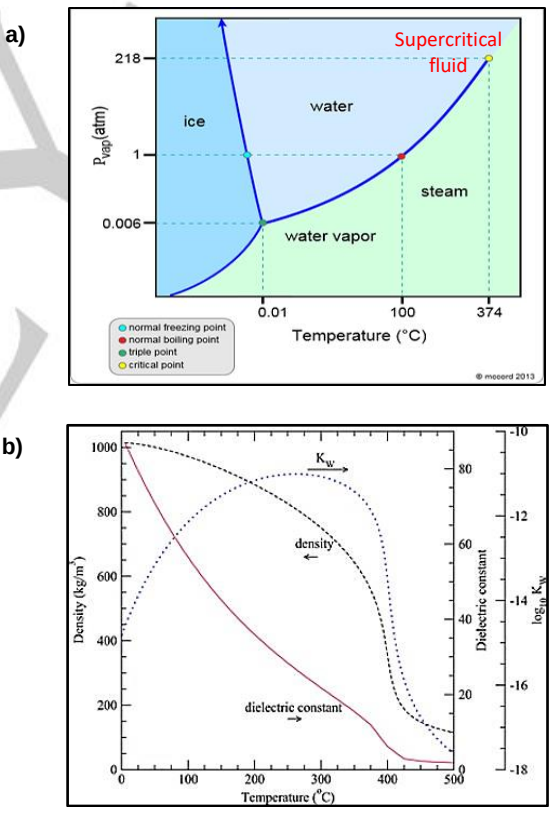

Fig. 5. (a) Phase diagram of water and (b) selected properties of supercritical water[23]

CHFS further facillitates the synthesis of 2D derivatives via bottom-up and top-down approaches. One step functionalisation with metal oxides/ metals as well as doping with hetero atoms can be easily achievable in producing 2D materials with superior properties.

b)

2.3.2. Continuous Hydrothermal Flow Reactor

In continuous hydrothermal flow system, there is an improved control of reaction temperature, pressure, residence time, precursor concentration and pH as well as the heating rate of precursors[23,59–61]. In the CHFS reactor, there are three feeds delivering precursors into the reactor that meet at the mixing point (**Reactor in Fig. 6)**. The first is a water feed **F1** which delivers water, pre-heated under set reaction temperature and pressure into the mixing point. The second feed **F2** meets at a **T**- junction with the third feed precursor **(Fig. 6)** before delivering its precursors (e.g. aqueous metal salt, graphene oxide etc.) to the mixing point. The third feed **P3** is called the auxiliary feed which supplies other required precursors e.g. surface stabilizers, alkaline solution etc.) to the mixing point. The resulting pressurized streams of precursors at the mixing point of the reactor are heated up rapidly with subsequent reaction occurring. The temperature of the mixing point as well as pressure and flow rates can be controlled which highlights one of the advantages of the continuous hydrothermal flow process[59]. After the resulting reaction, solution leaves the mixing point at the required residence time which depends on the flow rate of the feeds and tubing's diameter of the mixing point, the solution is cooled by a stream of cold water from the cooler at the base of the mixing point. The pressure of the reactor system is controlled by the back-pressure regulator (**BPR**) and the particles are collected from the outlet tubing of the BPR[61]. The particles are washed, separated by centrifugation and freeze-dried to obtain solid nanocrystals which are collected for analysis.

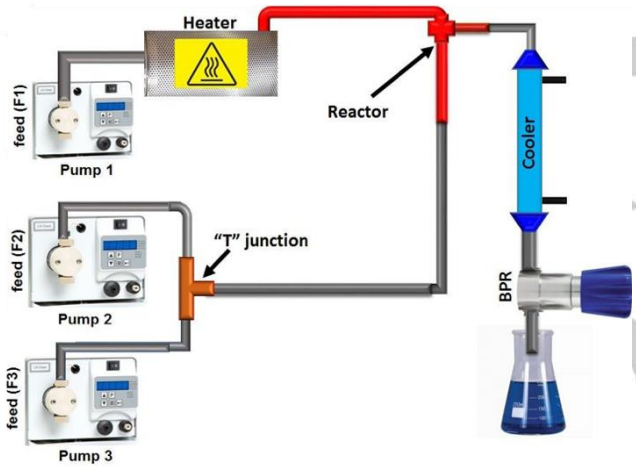

Fig.6. Schematic of CHFS process[62]

2.3.3. 2D Chemical Functionalisation via CHFS

In exploiting the physio-chemical properties of 2D materials, functionisation of material is vital to enable its processing through solvent-assisted techniques such as spin coating, filtration and layer-by-layer assembly[52], whilst maintaining their unique properties for several applications for example as integrals for next generation batteries, water treatment, bio-sensors and electronics. The key constraint for such applications is to produce and functionalise in a control mode, a high-quality 2D material with minimum defects utilizing a target-oriented approach (*i.e.* chemical and physical properties such as composition, structure, particle size and morphology are designed towards a specific target application).

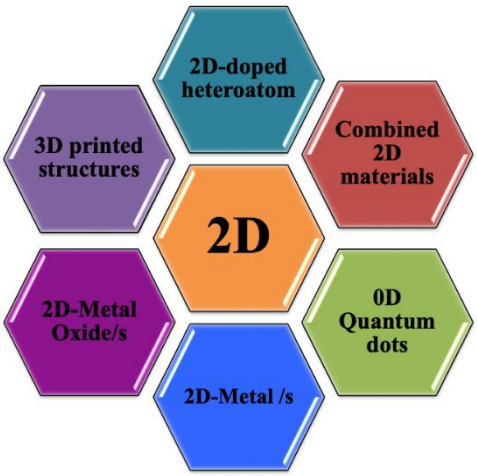

Fig. 7. Target materials[63]

This functionalisation can be achieved by covalent and non-covalent improvement techniques involving surface modification via chemical oxidation or reduction (e.g. reduced graphene oxide), doping (e.g. N and S- doped MXenes), addition of chemical groups (e.g. polymers), sonication and exfoliation to facilitate formation into sheets, stable dispersions and enhance their properties for numerous applications[52,64]. Surface functionalisation assists in tuning the properties of a material to achieve a specific function ranging from drug delivery to biosensing, energy storage and other applications[44,65,66]. Through this means, designing a range of functional 2D materials with superior properties from their parent 2D is feasible **(Fig. 7).**

Generally, the covalent functionalisation of nanomaterials involves addition of reactive molecules to the crystal lattice. For instance, the addtion of molecules to the conjugated π-system of its sp^2-carbon crystal lattice[67], creates negatively charged graphene sheets which increases coloumbic repulsion thereby improving its dispersion in solvents. This form of functionalisation introduces chemical activation due to reduction of chemical groups from both sides of graphene sheets[67]. Another technique of covalent functionalisation of 2D materials is doping as seen in nitrogen-doped MXenes[43] which involves insertion of impurities to the crystal lattice of a semiconductors to alter their properties. This involves insertion of either a donor impurity or acceptor impurity atom into the crystal lattice of the material[68].

Covalent functionalisation can be achieved hydrothermally via continuous flow processes to provide materials with diverse technological applications. Quality parameters such as surface defects, mechanical deformation and electronic environment as well as the number of 2D layers, (all induced as a result of the synthetic process), profoundly affect the end properties of the material. Novoselov and co-workers isolated graphene by mechanical exfoliation of graphite[69]. More synthetic techniques of graphene have been reported in literature which includes chemical vapour deposition (CVD), enhanced CVD via plasma, electric arc-discharge, epitaxial growth on electrically insulating surfaces, unzipping carbon nanotubes and chemical oxidation-reduction of graphite[52]. However, the best and most adopted technique by researchers have been the chemical oxidation-reduction of graphite referred to as the modified Hummer's method[70,71]. Herein, graphite is oxidised to graphene oxide (GO) whose surface is highly oxygenated with carboxyl, epoxyl, hydroxyl and ketone functional groups **(Fig. 8)**.

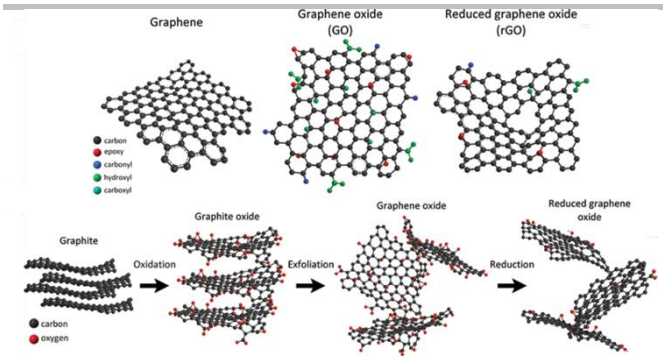

Fig. 8. Chemical structures of graphene and graphite derivatives via functionalisation[64]

However, the reduction of graphene oxide (rGO) to graphene is required to recover the conjugated network as well as superior properties, process which mainly involves the utilization of toxic and very unstable (potentially explosive) reducing agents, which also leave trace residues inducing deterioration in the performance of graphene material. Other synthetic routes have been developed, however despite these efforts, fine control and tuning of the properties of graphene sheets and graphene related nanomaterials still remains ongoing. In covalent functionalisation via CHFS (which introduces a greener process of synthesis and does not involve use of highly toxic chemicals but rather water-soluble precursors at supercritical conditions) was explored in research work by Kellici et al., (2014), where hazardous commercial chemicals such as hydrazine was replaced by potassium hydroxide (KOH) in the synthesis of reduced graphene oxide[59]. The fuctionalised 2D reduced grahene oxide was reported to have high antibacterial properties. This method offers a green, faster and economic synthetic means of graphene production with great controllability over oxygen functionalities as well as particle size by controlling the temperature, pressure and flow rate of the reaction as well as the concentration of the precursors[60].

CHFS, a single step synthetic route not only facilitates control over oxidation state of 2D nanomaterials but also offers an advantageous route for homogeneously producing and depositing highly crystalline nanostructures into 2D-materials (G, h-BN, MXene and MoS_2) and less explored 2D-nitrides/heteroatom.
The 2D platelike structure it offers an attractive substrate for deposition of inorganic nanoparticles for highly dispersed composites with novel properties. Thus, by feeding water dispersions of 2D material into a CHFS process at different points of nucleation (i.e. before nucleation and after or during nucleation), it will be possible to fully integrate these two materials into true nanocomposites. For instance, Kellici and co-workers also demonstrated a single rapid method of synthesising Ag-graphene nanocomposites with excellent antibacterial properties through combination with sulfonated calixarenes **(Fig. 9)**[72]. In their work, surface-functionalised reduced graphene oxide (rGO) through continuous hydrothermal flow method provides a support for Ag nanoparticles to prevent aggregation and also enhances bacteria adsorption due to negatively charged rGO surface. The Ag nanoparticles are stabilized by a class of macrocyclic compounds called calixarenes[72]. The nanocomposites showed high activity against E. coli (Gram-negative) and S. aureus (Gram-positive) bacteria and in selected cases the materials were reported to outperfom traditional antibiotics. Ceria-zirconia oxide/graphene nanocomposites were prepared via CHFS as a catalyst for the synthesis of dimethyl carbonate (DMC) from methanol and carbon dioxide[73] **(Fig. 10)**. In this work, graphene served as a substrate for growing ceria and zirconia oxide on its surface.

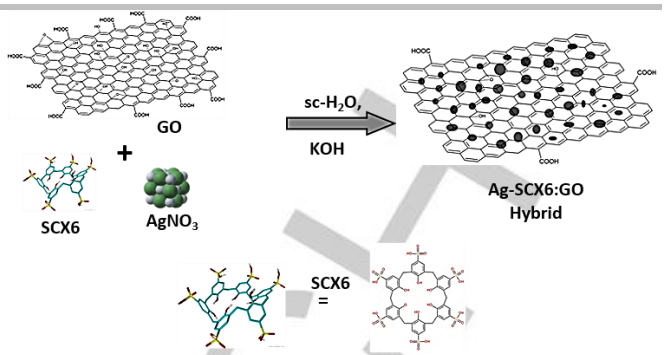

Fig. 9. Calixarene-assisted synthesis of Ag-graphene nanocomposites via CHFS[72]

The process modifies the surface of graphene and lowers its oxidation, resulting in the production of highly crystalline nanostructures. The synthesised ceria-zirconia oxide/graphene nanocomposites produced a 58% methanol conversion to generate a 33% yield of DMC[73]. This method produced 82.4% conversion of propylene carbonate (PC) and a DMC yield of 78.2%[73]. Tin doped zirconia (Zr–Sn–O) and tin doped zirconia/graphene nanocomposite (Zr–Sn/GO) have also been synthesised by CHFS as catalysts for the synthesis of DMC[31].

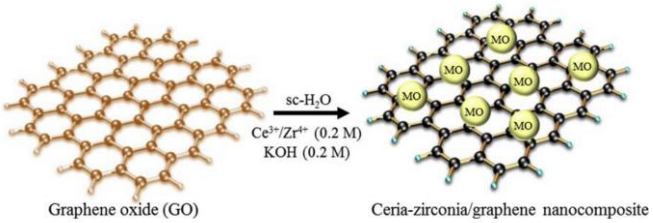

Fig. 10. Schematic of hydrothermal synthesis of Ce–Zr oxide/graphene nanocomposite catalyst[73]

CHFS materials portfolio also includes the first development of directly printed graphene based 3D structured heterogenous catalysts utilised for an industrially relevant reaction, the conversion of CO_2 into cyclic carbonates. Therein, 3D printed structures of CHFS synthesized graphene-based CeZrLa nanocatalyst showed improved activity with higher CO_2 conversion[74] **(Fig. 11.)**. The process involves utilisation of CO_2 in the presence of CHFS synthesised 2D based- 3D structured heterogeneous catalyst to directly produce propylene carbonate without the use of organic solvents. In addition, the nanocatalyst's ability to seperate from the product reduces materials and operating costs thereby contributing to the sustainability of the process[74]. This printing strategy shows great potential and fuels more pursuit towards green technology.

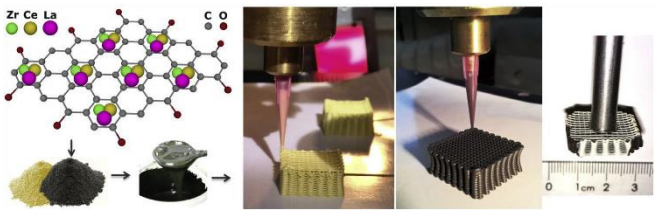

Fig. 11. Process of manufacture of nanocomposite structures including 3D printing of unsupported(mid-yellow image) and GO- supported CeZrLa structures[74]

Graphene has a zero-band gap due to its valence and conduction bands meet at the dirac points. This can be tuned through doping to facilitate its use in semiconductor electronic devices[68]. This insertion alters the crystal lattice parameter, creates conduction electrons and holes which are agents of conducting currents and therefore enhances the quality of the material for energy storage and opto-electronic applications. The zero-band gap of graphene can also be tuned by modifying graphene into nanoribbons, quantum dots and nanotubes where the resulting band gap is proportional to their respective widths. The optical properties of these 2D materials are reported to be size dependent and as such, control or tunability is needed. Surface modification also extend to particle size control; achieved by introduction of a particle size limiting agent on the surface of the 2D material. This modification affects the properties and potential application of the material. For example, in the CHFS of graphene quantum dots (GQDs) from graphene using calix [4] arene tetrasulfonic acid as a size limiting agent, highly stable and luminescent GQDs were obtained with tuned optical properties and bandgap due to reduced particle size[60]. The authors engineering the particle size via a range of molecular capping tools. This modification provides the material with exciting physical, chemical and optical properties that render its application in bio-tagging and bio-sensing. The hydrothermal fragmentation of graphene sheets was further explored using calix[4] arene tetraphosphonic acid (PCX4). This route allowed the surface functionalisation of GO to synthesize GQDs with controlled and enhanced optical properties **(Fig.12)**[61].

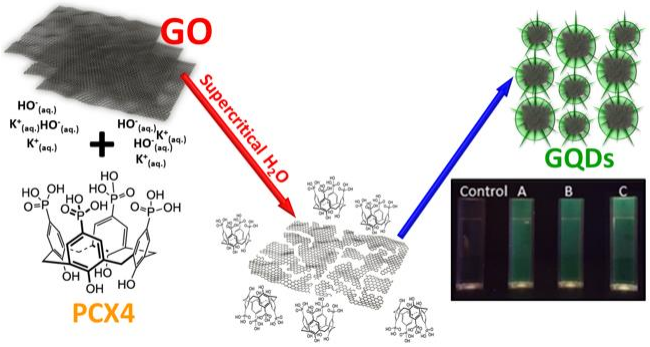

Fig. 12. Schematic of GQDs synthesis with PCX4[61]

Further, recent developments highlight a CHFS approach that directly obtains in a continuous manner luminescent graphitic core carbon quantum dots (CQD) using targeted simple precursors: citric acid and ammonia. This class of materials (0D quantum dots) have been gaining global interest as they have proven applications in photovoltaic and catalytic systems such as hydrogen and oxygen evolution as well as energy storage. In this work, the authors show that the specific nanostructured carbon produced can be effective in a sensor that selectively detects Cr(VI) a toxic cation found in many developing countries as a by-product of poorly regulated industry. The materials were reported to have an average particle size of 3.3 ± 0.7 nm, nitrogen-doped, blue luminiscent exhibiting rarely observed excitation independent properties.

Above and beyond batch or continuous flow addition processes, surface functionalisation of nanoparticles can also be achieved through sonication-induced exfoliation of materials in the presence of surface modifying agents. This was demonstrated in research work carried out by Vaughn and co-workers where surface-functionalised MXenes were synthesised by selective calixarene-assisted delamination of Ti_2C into various morphologies including, plates, spheres, scrolls and sheets **(Fig. 13a-d** respectively**)**[75].

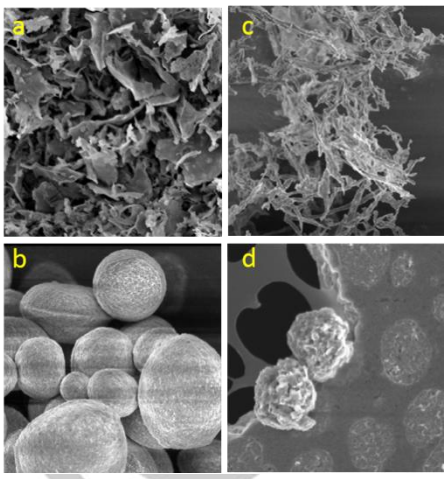

Fig. 13. MXene morphologies in the presence of calixarenes[75]

3. Advantages of CHFS over Batch Hydrothermal Synthesis (BHS)

Batch hydrothermal synthesis (BHS) involves a slow reaction process (several hours or days) as compared to Continuous Hydrothermal Flow Synthesis (CHFS) which produces materials through a faster reaction time by passing water-soluble precursors through a stream of supercritical water[60]. CHFS reaction times are in the order of seconds or fractions of a second, and indeed, the time from precursor to recovered nanomaterial (at the exit of the process) is in the order of a couple of minutes typically. This reaction time determines the extent of nucleation and the sizes of particles formed at the end of the process. Moreover, the reaction temperature when the two flows are mixed is typically in the range of 300–380 °C, compared to typically less than 250°C for batch hydrothermal. Thus, CHFS synthesis/functionalisation occurs at supercritical conditions where the reaction rate increases due to a decrease in the dielectric constant of supercritical water[76]. Fine particles, metal oxides and single crystals can be synthesised in CHFS by processing in near- critical or supercritical water conditions by controlling the density, viscosity and dielectric constant of the reaction medium through independent control over reaction parameters such as flow rates, temperature and pressure[59]. Through this means, there is an ease to tune the particle size, morphology and crystal structure of as-synthesised materials (unlike BHS where larger particle sizes are obtained). In addition, CHFS provides an environmentally stable production route of nanomaterials from resource extraction to the factory gate. This is evident in the life-cycle assessment (LCA) of nano-TiO_2 production via CHFS to assess its environmental impacts[77]. LCA results were generated using Simapro 8.0.4 and environmental impacts were calculated on the basis of cumulative energy demand and global warming potential which ranges from 75 to 110 MJ kg^{-1} indicating CHFS as an energy-efficient nanomaterial production process[77,78]. CHFS technology has further shown its green nature in the synthesis of nanomaterials by replacing organic solvents and compounds requiring energy intense processing and generate higher emissions with water as a solvent resulting in lower emissions in raw materials and post-processing techniques[77]. Kellici et.al (2018) performed a LCA analysis in the CHFS of GQDs using SimaPro (8.3.0.0) software with Ecoinvent 3 Life Cycle Inventory database. Conclusions from this LCA analysis showed that CHFS generates significant degree of reduction in the overall life-cycle environmental impact when compared to batch hydrothermal method.

Hence, CHFS provides numerous advantages over batch hydrothermal *via* providing a rapid (nanomaterials generated in few seconds), green (utilises water rather than toxic precursors), low cost, scalable, efficient, continuous and reproducible procedure of synthesising high surface area and highly crystalline nanomaterials (**Fig .14)**.

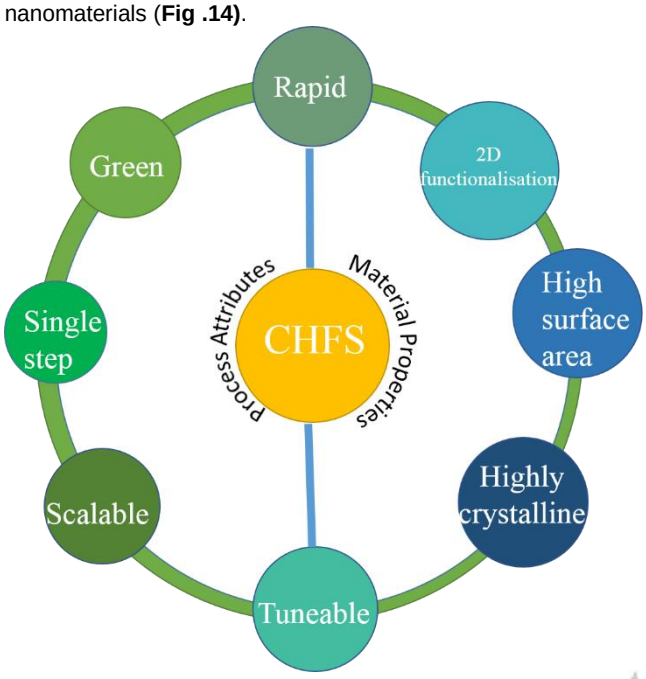

Fig. 14. Advantages of CHFS approach in material synthesis and the properties of the materials that it offers

4. Conclusions and Outlook

The use of hydrothermal flow methodologies for the synthesis of inorganic nanomaterials has made a significant contribution in material science and engineering. Advantages of producing nanomaterials via controlling reaction parameters are evident. Hydrothermally synthesised materials exhibit extremely high surface areas and crystallinity, with possible chemical functionalisation for much improved properties for several applications and processing into solutions. Generating functionalities in these materials are essential in exploring their intrinsic properties which they offer in a wide range of applications. BHS of these nanomaterials consumes more time, energy and involves use of hazardous chemicals to produce large size particles. As a result, CHFS offers an ease in the process of synthesis, surface and chemical modification of these nanomaterial by providing control over reaction parameters such as temperature, pressure, precursor concentration and residence time to synthesise, tailored materials for several applications in short-range time (a few seconds). Certainly, there is plenty of scope for further explorations and the next decade or so will see the continuous hydrothermal route playing a greater role towards chemical functionalisation of 2D materials.

CHFS is a unique solution delivering (in collaboration with other disciplines) world-class material engineering by facilitating a gold access path in integrating 2D active functional materials across a broad range of potential applications aiming to solve global challenges including energy storage (electrode for lithium ion batteries, supercapacitors and solar cells), CO_2 reduction and other environmental pollutants (catalyst/absorber), biomedical (antibacterial, biosensors and bio-tagging) and beyond.

This rapid, clean, rapid and novel technology will enable a step change in the cost, performance and durability (due to the high throughput and comparatively lower cost of the process combined with the tighter control of chemical and physical properties of the materials). This step change will have cascading effects in industry (through access to next generation high tech components), academia (through the access to a range of new industry led research areas surrounding these applications), and wider society as a whole (through both the economic growth of led by our high tech industry, and through the solutions to societal, economic, and environmental problems that result from these 2D nanocomposites being integrated into new technologies).

Acknowledgements

We would like to acknowledge London South Bank University for the continued support rendered to authors in helping to develop research and make significant contributions to this review. Big thank you goes to all collaborators.

Fig. 2. adapted from Ref. 6, Ref. 10, and Ref.11 with permission from American Chemical Society (ACS)
Fig. 9. reprinted with permission from S. Kellici, J. Acord, A. Vaughn, N. P. Power, D. J. Morgan, T. Heil, S. P. Facq and G. I. Lampronti, *ACS Appl. Mater. Interfaces*, 2016, **8**, 19038–19046**.**
Fig. 11. reprinted from, Apllied Catalysis B: Environmental Volumes 168–169, , R. Saada, S. Kellici, T. Heil, D. Morgan and B. Saha, Greener synthesis of dimethyl carbonate using a novel ceria–zirconia oxide/graphene nanocomposite catalyst, June 2015, Pages 353-362., Copyright (2015), with permission from Elsevier
Fig. 3. reproduced from R. Younas, S. Hao, L. Zhang and S. Zhang, *Renew. Energy*, 2017, **113**, 532–545 has been cited and referenced accordingly in this article to validate permission to reuse.
Fig. 5. reprinted with permission from P. W. Dunne, A. S. Munn, C. L. Starkey, T. A. Huddle and E. H. Lester, *Philos. Trans. R. Soc. A Math. Phys. Eng. Sci*., 2015, **373**, 20150015.
Permissions of reuse/ adaptation of other figures that are used in this article have been requested and granted.

References

1 H. Zhang, *ACS Nano*, 2015, **9**, 9451–9469.
2 A. Jayakumar, A. Surendranath and M. PV, *Int. J. Pharm.*, 2018, **551**, 309–321.
3 C. Tan, X. Cao, X. J. Wu, Q. He, J. Yang, X. Zhang, J. Chen, W. Zhao, S. Han, G. H. Nam, M. Sindoro and H. Zhang, *Chem. Rev.*, 2017, **117**, 6225–6331.
4 J. He, L. Tao, H. Zhang, B. Zhou and J. Li, *Nanoscale*, 2019, **11**, 2577–2593.
5 B. Anasori, M. R. Lukatskaya and Y. Gogotsi, *Nat. Rev. Mater.*, 2017, **2**, 16098.
6 Q. Tang and D. E. Jiang, *Chem. Mater.*, 2015, **27**, 3743–3748.
7 K. Huang, Z. Li, J. Lin, G. Han and P. Huang, *Chem. Soc. Rev.*, 2018, **47**, 5109–5124.
8 J. Zhao, H. Liu, Z. Yu, R. Quhe, S. Zhou, Y. Wang, C. C. Liu, H. Zhong, N. Han, J. Lu, Y. Yao and K. Wu, *Prog. Mater. Sci.*, 2016, **83**, 24–151.
9 J. Wang, F. Ma and M. Sun, *RSC Adv.*, 2017, **7**, 16801–16822.
10 T. Hussain, T. Kaewmaraya, S. Chakraborty, H. Vovusha, V. Amornkitbamrung and R. Ahuja, *ACS Sensors*, 2018, **3**, 867–874.
11 S. Geng, L. Wu, H. Cui, W. Tan, T. Chen, P. K. Chu and X. F. Yu, *Chem. Commun.*, 2018, **54**, 6060–6063.
12 E. V. Castro, H. Ochoa, M. I. Katsnelson, R. V. Gorbachev, D. C. Elias, K. S. Novoselov, A. K. Geim and F. Guinea, *Phys. Rev. Lett.*, 2010, **105**, 266601–266605.
13 Y. Han, Y. Ge, Y. Chao, C. Wang and G. G. Wallace, *J. Energy Chem.*, 2018, **27**, 57–72.
14 C. J. Zhang, M. P. Kremer, A. Seral-Ascaso, S. H. Park, N. McEvoy, B. Anasori, Y. Gogotsi and V. Nicolosi, *Adv. Funct. Mater.*, 2018, **28**, 1705506.
15 Z. He and W. Que, *Appl. Mater. Today*, 2016, **3**, 23–56.

16 P. Afanasiev, G. F. Xia, G. Berhault, B. Jouguet and M. Lacroix, *Chem. Mater.*, 1999, **11**, 3216–3219.
17 J. Wang, G. Li and L. Li, *Two-dimensional Mater. - Synth. Charact. Potential Appl.*, 2016, 1–17.
18 G. Liu, J. Cui, R. Luo, Y. Liu, X. Huang, N. Wu, X. Jin, H. Chen, S. Tang, J. K. Kim and X. Liu, *Appl. Surf. Sci.*, 2019, **469**, 854–863.
19 P. W. Dunne, A. S. Munn, C. L. Starkey and E. H. Lester, *Chem. Commun.*, 2015, **51**, 4048–4050.
20 M. Naguib, M. Kurtoglu, V. Presser, J. Lu, J. Niu, M. Heon, L. Hultman, Y. Gogotsi and M. W. Barsoum, *Adv. Mater.*, 2011, **23**, 4248–4253.
21 J. Yan, C. E. Ren, K. Maleski, C. B. Hatter, B. Anasori, P. Urbankowski, A. Sarycheva and Y. Gogotsi, *Adv. Funct. Mater.*, 2017, **27**, 1701264.
22 Z. Fan, Y. Wang, Z. Xie, D. Wang, Y. Yuan, H. Kang, B. Su, Z. Cheng and Y. Liu, *Adv. Sci.*, 2018, **5**, 18000750.
23 P. W. Dunne, A. S. Munn, C. L. Starkey, T. A. Huddle and E. H. Lester, *Philos. Trans. R. Soc. A Math. Phys. Eng. Sci.*, 2015, **373**, 20150015.
24 R. Kurapati, K. Kostarelos, M. Prato and A. Bianco, *Adv. Mater.*, 2016, **28**, 6052–6074.
25 K. Byrappa and M. Yoshimura, in *Handbook of Hydrothermal Technology*, 2013, pp. 1–81.
26 K. Byrappa and T. Adschiri, *Prog. Cryst. Growth Charact. Mater.*, 2007, **53**, 117–166.
27 V. Middelkoop, C. J. Tighe, S. Kellici, R. I. Gruar, J. M. Perkins, S. D. M. Jacques, P. Barnes and J. A. Darr, *J. Supercrit. Fluids*, 2014, **87**, 118–128.
28 Y. Hakuta, H. Hayashi and K. Arai, *Curr. Opin. Solid State Mater. Sci.*, 2003, **7**, 341–351.
29 R. Younas, S. Hao, L. Zhang and S. Zhang, *Renew. Energy*, 2017, **113**, 532–545.
30 A. A. Galkin, B. G. Kostyuk, N. N. Kuznetsova, A. O. Turakulova, V. V. Lunin and M. Polyakov, *Kinet. Catal.*, 2001, **42**, 154–162.
31 R. Saada, O. AboElazayem, S. Kellici, T. Heil, D. Morgan, G. I. Lampronti and B. Saha, *Appl. Catal. B Environ.*, 2018, **226**, 451–462.
32 W. Wang, H. Lin, J. Li and N. Wang, *J. Am. Ceram. Soc.*, 2008, **91**, 628–631.
33 W. J. Niu, Y. Li, R. H. Zhu, D. Shan, Y. R. Fan and X. J. Zhang, *Sensors Actuators, B Chem.*, 2015, **218**, 229–236.
34 Z. Wang, Y. Hu, W. Wang, D. Zhou, Y. Wang and H. Gu, in *Integrated Ferroelectrics*, 2013, pp. 24–30.
35 L. Ze, G. Yueqiu, L. Xujun and Z. Yong, *Appl. Surf. Sci.*, 2017, **399**, 330–336.
36 Z. Wu, L. Xie, Y. Xiao and D. Wang, *J. Alloys Compd.*, 2017, **708**, 763–768.
37 B. Qiu, M. Xing and J. Zhang, *J. Am. Chem. Soc.*, 2014, **136**, 5852–5855.
38 J. W. Lee, A. S. Hall, J. D. Kim and T. E. Mallouk, *Chem. Mater.*, 2012, **24**, 1158–1164.
39 G. Huang, T. Chen, W. Chen, Z. Wang, K. Chang, L. Ma, F. Huang, D. Chen and J. Y. Lee, *Small*, 2013, **9**, 3693–3703.
40 L. Q. Fan, G. J. Liu, C. Y. Zhang, J. H. Wu and Y. L. Wei, *Int. J. Hydrogen Energy*, 2015, **40**, 10150–10157.
41 G. He, M. Qiao, W. Li, Y. Lu, T. Zhao, R. Zou, B. Li, J. A. Darr, J. Hu, M. M. Titirici and I. P. Parkin, *Adv. Sci.*, 2017, **4**, 1–10.
42 Z. Yang, Z. Yao, G. Li, G. Fang, H. Nie, Z. Liu, X. Zhou, X. Chen and S. Huang, *ACS Nano*, 2012, **6**, 205–211.
43 L. S. Panchakarla, K. S. Subrahmanyam, S. K. Saha, A. Govindaraj, H. R. Krishnamurthy, U. V. Waghmare and C. N. R. Rao, *Adv. Mater.*, 2009, **21**, 4726–4730.
44 Y. Wen, T. E. Rufford, X. Chen, N. Li, M. Lyu, L. Dai and L. Wang, *Nano Energy*, 2017, **38**, 368–376.
45 C. Peng, P. Wei, X. Chen, Y. Zhang, F. Zhu, Y. Cao, H. Wang, H. Yu and F. Peng, *Ceram. Int.*, 2018, **44**, 18886–18893.
46 F. Han, S. Luo, L. Xie, J. Zhu, W. Wei, X. Chen, F. Liu, W. Chen, J. Zhao, L. Dong, K. Yu, X. Zeng, F. Rao, L. Wang and Y. Huang, *ACS Appl. Mater. Interfaces*, 2019, **11**, 8443–8452.
47 J. C. Lei, X. Zhang and Z. Zhou, *Front. Phys.*, 2015, **10**, 276–286.
48 Y. Dong, Z. S. Wu, S. Zheng, X. Wang, J. Qin, S. Wang, X. Shi and X. Bao, *ACS Nano*, 2017, **11**, 4792–4800.
49 W. Gu, Y. Yan, C. Zhang, C. Ding and Y. Xian, *ACS Appl. Mater. Interfaces*, 2016, **8**, 11272–11279.
50 D. Pan, J. Zhang, Z. Li and M. Wu, *Adv. Mater.*, 2010, **22**, 734–738.
51 Q. Xu, L. Ding, Y. Wen, W. Yang, H. Zhou, X. Chen, J. Street, A. Zhou, W. J. Ong and N. Li, *J. Mater. Chem. C*, 2018, **6**, 6360–6369.
52 T. Kuila, S. Bose, A. K. Mishra, P. Khanra, N. H. Kim and J. H. Lee, *Prog. Mater. Sci.*, 2012, **57**, 1061–1105.
53 C. Shan, H. Yang, D. Han, Q. Zhang, A. Ivaska and L. Niu, *Langmuir*, 2009, **25**, 12030–12033.
54 Y. Gogotsi, J. A. Libera and M. Yoshimura, *J. Mater. Res.*, 2000, **15**, 2591–2594.
55 N. T. K. Thanh and L. A. W. Green, *Nano Today*, 2010, **5**, 213–230.
56 E. Lester, P. Blood, J. Denyer, D. Giddings, B. Azzopardi and M. Poliakoff, *J. Supercrit. Fluids*, 2006, **37**, 209–214.
57 A. J. Hunt and T. M. Attard, *Supercritical and Other High-pressure Solvent Systems*, Royal Society of Chemistry, Cambridge, 2018.
58 J. A. Darr, J. Zhang, N. M. Makwana and X. Weng, *Chem. Rev.*, 2017, **117**, 11125–11238.
59 S. Kellici, J. Acord, J. Ball, H. S. Reehal, D. Morgan and B. Saha, *RSC Adv.*, 2014, **4**, 14858–14861.
60 S. Kellici, J. Acord, N. P. Power, D. J. Morgan, P. Coppo, T. Heil and B. Saha, 2017, **7**, 14716–14720.
61 S. Kellici, J. Acord, K. E. Moore, N. P. Power, V. Middelkoop, D. J. Morgan, T. Heil, P. Coppo, I. A. Baragau and C. L. Raston, *React. Chem. Eng.*, 2018, **3**, 949–958.
62 I.-A. Baragau, N. P. Power, D. J. Morgan, T. Heil, R. A. Lobo, C. S. Roberts, M. Titirici, S. Dunn and S. Kellici, *J. Mater. Chem. A*, 2020.
63 Continuous Hydrothermal Flow Synthesis | nano2d, https://www.nano2d.co.uk/continuous-hydrothermal-flow-synthe, (accessed 3 January 2020).
64 E. Jimenez-Cervantes, J. López-Barroso, A. L. Martínez-Hernández and C. Velasco-Santos, in *Recent Advances in Graphene Research*, 2016, pp. 258–287.
65 H. Rui, R. Xing, Z. Xu, Y. Hou, S. Goo and S. Sun, *Adv. Mater.*, 2010, **22**, 2729–2742.
66 S. Vardharajula, S. Z. Ali, P. M. Tiwari, E. Eroğlu, K. Vig, V. A. Dennis and S. R. Singh, *Int. J. Nanomedicine*, 2012, **7**, 5361–5374.
67 G. Bottari, M. Ángeles Herranz, L. Wibmer, M. Volland, L. Rodríguez-Pérez, D. M. Guldi, A. Hirsch, N. Martín, F. D'Souza and T. Torres, *Chem. Soc. Rev.*, 2017, **46**, 4464–4500.
68 H. Liu, Y. Liu and D. Zhu, *J. Mater. Chem.*, 2011, **21**, 3335–3345.
69 K. S. Novoselov, A. K. Geim, S. V. Morozov, D. Jiang, Y. Zhang, S. V. Dubonos, I. V. Grigorieva and A. A. Firsov, *Science (80-.).*, 2004, **306**, 666–669.
70 Y. Hernandez, V. Nicolosi, M. Lotya, F. M. Blighe, Z. Sun, S. De, I. T. McGovern, B. Holland, M. Byrne, Y. K. Gun'ko, J. J. Boland, P. Niraj, G. Duesberg, S. Krishnamurthy, R. Goodhue, J. Hutchison, V. Scardaci, A. C. Ferrari and J. N. Coleman, *Nat. Nanotechnol.*, 2008, **3**, 563–568.
71 D. C. Marcano, D. V. Kosynkin, J. M. Berlin, A. Sinitskii, Z. Sun, A. Slesarev, L. B. Alemany, W. Lu and J. M. Tour, *ACS Nano*, 2010, **4**, 4806–4814.
72 S. Kellici, J. Acord, A. Vaughn, N. P. Power, D. J. Morgan, T. Heil, S. P. Facq and G. I. Lampronti, *ACS Appl. Mater. Interfaces*, 2016, **8**, 19038–19046.
73 R. Saada, S. Kellici, T. Heil, D. Morgan and B. Saha, *Appl. Catal. B Environ.*, 2015, **168–169**, 353–362.
74 V. Middelkoop, T. Slater, M. Florea, F. Neaţu, S. Danaci, V. Onyenkeadi, K. Boonen, B. Saha, I. A. Baragau and S. Kellici, *J. Clean. Prod.*, 2019, **214**, 606–614.
75 A. Vaughn, J. Ball, T. Heil, D. J. Morgan, G. I. Lampronti, G. Maršalkaitė, C. L. Raston, N. P. Power and S. Kellici, *Chem. - A Eur. J.*, 2017, **23**, 8128–8133.
76 M. Claverie, M. Diez-Garcia, F. Martin and C. Aymonier, *Chem. - A Eur. J.*, 2019, **25**, 5814–5823.
77 P. Caramazana-González, P. W. Dunne, M. Gimeno-Fabra, M. Zilka, M. Ticha, B. Stieberova, F. Freiberg, J. McKechnie and E. H. Lester, *Green Chem.*, 2017, **19**, 1536–1547.
78 S. Middlemas, Z. Z. Fang and P. Fan, *J. Clean. Prod.*, 2015, **89**, 137–147.

10.1002/chem.202000383